IAC-06-B6.1.1

PERFORMANCE OF A PROPOSED INSTRUMENT FOR SPACE-BASED OPTICAL OBSERVATIONS OF SPACE DEBRIS

T. Flohrer

Astronomical Institute, University of Bern, CH-3012 Bern, Switzerland
tim.flohrer@aiub.unibe.ch

T. Schildknecht[1], R. Jehn[2], M. Oswald[3]

[1]Astronomical Institute, University of Bern, CH-3012 Bern, Switzerland
thomas.schildknecht@aiub.unibe.ch
[2]European Space Operations Centre, 64293 Darmstadt, Germany
ruediger.jehn@esa.int
[3]Institute of Aerospace Systems, TU Braunschweig, 38108 Braunschweig, Germany
m.oswald@tu-bs.de

ABSTRACT

In 2003, the European Space Agency (ESA) initiated a study entitled "Space-Based Optical Observation of Space Debris" in order to investigate means that would allow closing the knowledge gap for small-sized space debris objects. The study defined user requirements, developed an observation strategy for a space-based instrument capable of observing uncatalogued small-sized debris objects, and finally presented an instrument architecture and an operations concept for the passive optical observation of space debris objects in Low-Earth Orbit (LEO) and Geostationary Orbit (GEO). The object detection will be carried out on-board, while the astrometric reduction, orbit determination, and estimation of the size of objects are part of the on-ground processing. First orbits must be determined from a single observed crossing through the field of view. The proposed instrument combines a 20 cm aperture folded Schmidt telescope and a four megapixel, fast read-out camera using either a frame-transfer charge coupled device or a hybrid visible silicon imager sensor. This paper focuses on the detailed estimation of the system performance of that proposed instrument. We discuss the observable objects using the statistical reference population from ESA's MASTER-2005 model, as well as the main parameters that limit the possibility of the detection of objects. Based on simulations we evaluate the proposed object detection algorithm and the orbit determination. We conclude that in LEO ground-based radars are theoretically superior, but due to their limited availability a space-based system could still contribute significantly to the monitoring of the space debris environment. At GEO altitude the system could enhance the knowledge by decreasing the minimum object size from about 15 cm to less than 5 cm. The proposed instrument would allow improving the knowledge of the uncatalogued small-sized space debris population in LEO and GEO by using a simple instrument design and a straight-forward processing strategy.

INTRODUCTION

Today, space operators, satellite manufactures and mission designers are aware of the increasing risks due to the population of space debris objects in space. Through the development of space debris environment models, space agencies support the risk assessments that are undertaken during mission analysis and operation. An example is ESA's MASTER model that became upgraded to version 2005 recently. The development of sophisticated and reliable models does, however, rely on the availability of measurements that cover the entire space debris population. A continuous "flow" of space debris observations is needed, which provides significant spatial coverage and covers all diameters of the objects.

For space debris model development and validation, larger objects are sufficiently covered by Radar observations of the Low-Earth Orbit (LEO), as well as by means of optical observations of the Geostationary Orbit (GEO). A considerable problem is the fact that current space debris observations show a coverage gap in the millimeter to centimeter size region for the LEO and in the millimeter to decimeter size region for the GEO. Those missing observations of small-sized space debris objects lead to a knowledge gap today.

The European Space Agency (ESA) initiated a study entitled "Space-Based Optical Observation of Space Debris" in 2003. The study goal was to investigate cost-efficient means that allow closing the gap for small-sized space debris objects, to define user requirements, to develop an observation strategy for a space-based instrument capable of observing uncatalogued small-sized debris objects, and finally to present an instrument architecture and an operations concept. ESA required the proposed system to be capable to determine (at least statistically) orbits of the small-sized space debris objects in LEO and GEO by purely passive optical means.

The study was awarded to a study team led by the Finnish company ASRO (Aboa Space Research Oy, Turku). The National Aerospace Laboratory (NLR) from The Netherlands and the Astronomical Institute of the University of Berne (AIUB), Switzer-

land, completed the study team. The study finished with the presentation of the final report [1] in 2005. A previous paper [2] already presented the proposed sensor architecture for the space-based optical observation of space debris in a detailed manner. Another paper [3] reported on the observations concept.

In this paper the results are presented of a more refined, additional performance estimation that was carried out at the AIUB after the study had finished. This analysis is based on the selected sensor architecture and observation strategy without any modification. The baseline is presented in the first chapter, while in the second chapter the various system performance issues are addressed. Namely, we analyze the simulated observations using a statistical population of space debris objects from ESA's "Meteoroid and Space Debris Terrestrial Environment Reference Model" (MASTER) together with the accompanying "Program for Radar and Optical Observation Forecasting" (PROOF) in the new version 2005. The analysis is completed by the evaluation of the performance of image processing and orbit determination. We make use of newly introduced functionalities in PROOF's recent version that directly provide the required input for the orbit determination analysis.

SENSOR BASELINE AND OBSERVATION STRATEGY

For cost-efficiency reasons only fixed-mounted telescopes were considered in the study. The sensor is required to provide all measurements that are needed for orbit determination and the estimation of the size of objects from a single crossing of a particular object through the sensor field of view (FoV). To reduce the system requirements (mainly to limit the amount of transmitted data), the data processing must be split between on-board and on-ground processing. Object detection of both, reference stars and debris objects (and discrimination), will be carried out on-board, while the astrometric reduction, orbit determination and size estimation are part of the on-ground processing.

It was found that identical instruments might provide sufficient radiometric performance for both operating scenarios, LEO and GEO. Nevertheless, to ensure sufficient system performance the range to the small-sized objects must be short. Thus space debris objects orbiting in LEO need to be observed from a sensor in LEO, while space debris in GEO must be covered by observations acquired from a platform in the GEO vicinity.

For the LEO region the study proposes a sensor mounted on a satellite orbiting in a nearly circular sun-synchronous orbit of about 800 km altitude, close to the terminator plane. The line-of-sight (LOS) shall be oriented away from the Sun, mostly perpendicular to the orbital plane, but slightly inclined (see Figure 1). For the GEO region two concepts were studied. The first concept assumes utilization of the sensor mounted on a dedicated spacecraft that is in a low inclined circular orbit 1000 km below the GEO, a so-called subGEO orbit. In this case the pointing concept is proposed to be away from the Sun (see Figure 2). In the second concept the sensor is mounted as a secondary payload onto a GEO satellite, with the instrument LOS mostly perpendicular to the orbital plane, pointing to the North or to the South, but slightly inclined (see Figure 3). The LOS orientation in LEO and subGEO leads to optimal phase angle conditions (close to 0°), while the LOS orientation in GEO gives average phase angle of about 90°.

PERFORMANCE EVALUATION

Various groups carried out assessments on the possibility and performance of the space-based optical observation of space debris in the past [1], [4], [5], [6], [7], [8].

The only operational space-based optical sensor, the Space-Based Visible (SBV) on-board the US Midcourse space experiment is a space surveillance sensor and is not designed to search for small-sized space debris. The SBV technology, the operation concept and a functional demonstration are described in [9] and [10].
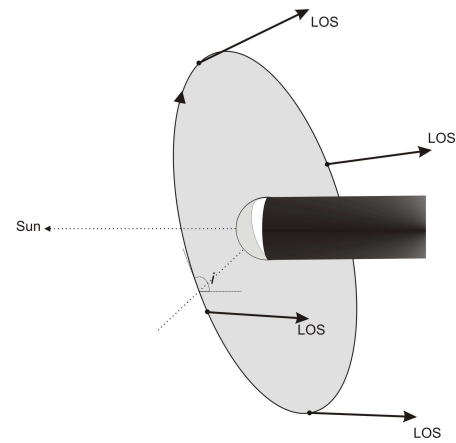
Fig. 1: LEO operational concept: placed in a sun-synchronous orbit close to the terminator, the LOS of the sensor is slightly inclined against the normal of the orbital plane, ensuring a pointing into densely populated regions in LEO.
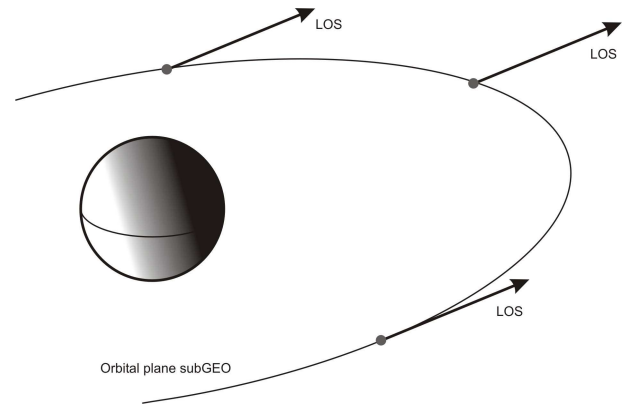
Fig. 2: SubGEO operational concept: a dedicated spacecraft in a near-circular, slightly inclined orbit below GEO, the LOS of the sensor is oriented away from the Sun.
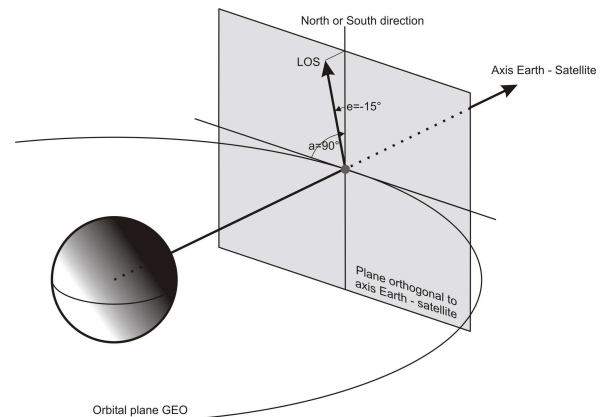
Fig. 3: GEO operational concept: mounted as secondary payload on-board a GEO satellite, the LOS of the sensor points to the North or South, but slightly inclined towards the Earth.

3

Based on results of ESA's PROOF tool Krag et al. [11], [12] presented a concept for optical observations from a sensor in a sun-synchronous orbit (SSO), from a near-GEO drifting orbit, and from a Geostationary Transfer orbit (GTO). In [13] orbit determination from a space-based platform is discussed. These early studies introduced PROOF as an extremely valuable tool for observation forecasting and performance evaluation of space-based observations, but did not focus on the technical feasibility of the proposed system architecture and processing concept.

The findings of the recent study "Space-Based Optical Observation of Space Debris" (SBO) [1] indicate that the sensor considered in the previous studies (a 381 mm aperture telescope with 6.8° FoV, combined with a 4096 pixel sensor in [13]) is extremely demanding, mainly in terms of the optical design, telescope weight and stability, and size of the focal plane. The proposed GTO strategy utilizing an Ariane 5 piggy-back launch demands radiation-hardened detectors, which would lower the detection efficiency significantly.

The instrument proposed in the SBO study combines a 20 cm aperture folded Schmidt telescope, a four megapixel, fast read-out camera using either a frame-transfer charge coupled device (CCD) or an Hybrid Visible Silicon Imager (HyViSI) sensor. With a focal length of 41 cm, the FoV diameter is 6°. For a detailed sensor description we refer to the previous publications on the SBO sensor conceptual architecture and design [2], [3].

It is worth to mention that in the current paper we present a performance evaluation including radiometry, image processing, and orbit determination aspects. The performance of the proposed system is evaluated in three steps. In a first step we discuss the observable objects using a statistical reference population from ESA's MASTER-2005 model [17] with the help of the observation-forecasting tool PROOF-2005 [18]. Using the obtained characteristics of objects crossing the FoV, we discuss the main parameters that limit the detection of objects. The next step is the analysis of the proposed image processing algorithm on-board. Finally, in the last step, the orbit determination of the detectable space debris population is evaluated.

Assessment of the observable objects using PROOF

We used ESA's PROOF-tool in its new version 2005 for the estimation of the number and the characteristics of FoV crossing events. The FoV crossing events were generated by PROOF from a statistical reference population of space debris objects, which is the ESA MASTER-2005 population. PROOF-2005 was used in the "statistic mode", and the reference epoch was 2005-05-01. To save computing time, the minimum object diameter was set to 5 mm, and the considered ranges were limited to 10000 km. Furthermore, we combined the results from four Monte Carlo runs covering 24 h of observation time each, in order to improve the statistics. The PROOF-runs were executed for the 6th and 21st day of each month, over a one-year period starting December 2005. This altogether covers 576 h of simulated observation time. It must be kept in mind that all presented numbers are strongly dependent on the underlying space debris population model.

As it was found that the results for CCD-detectors do not differ significantly from the HyViSI-detector results [1], we will only present the results for the HyViSI detector here.

Far more important for the interpretation of the simulation results is the considered observation range. Due to CPU-time limitations only a limited band of observation ranges can be simulated. The main focus of the SBO sensor is on small-sized space debris objects. As the detection performance is expected better for short ranges to the objects, the lower limit is 0 km, while for the upper bound we used for all operation scenarios 10000 km.

In LEO there is, however, a significant loss in detection sensitivity for increasing ranges. Figure 4 shows the peak signal-to-noise ratio (SNR) as function of the object diameter for five selected range bands. In the following, we will always refer to the peak SNR per single pixel. Figure 4 indicates that for a reasonable SNR>3 a significant number of detectable FoV crossing events of small-sized space debris objects (<0.1 m) can only be expected for ranges below about 400 km.
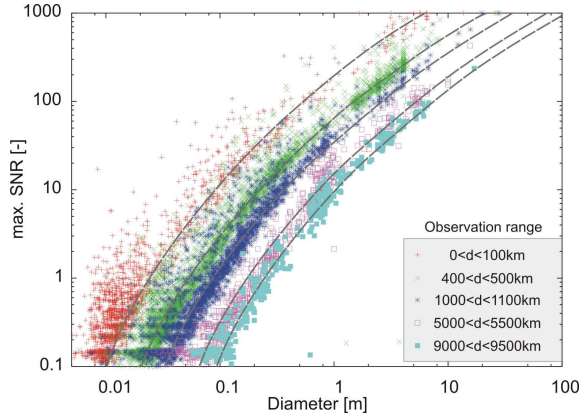
Fig. 4: Peak SNR per pixel as function of the object diameter in the LEO concept for five selected data subsets with different bands of the observation range. The dashed lines indicate the average of the corresponding data subset.

The FoV dwell time is significantly shorter for short-range FoV crossings, but for small objects the increase of the SNR due to the shorter range exceeds the decrease of the SNR due to the higher FoV crossing velocity. The comparison of the FoV dwell time with the observation range in Figure 5 shows that for observation ranges below 500 km the FoV dwell time is typically between 0.4 and 5 s. For the long-range observations, dwell times of several minutes are possible. Dwell times below 10 s must be understood as demanding in terms of acquiring the required number of position measurements. Due to this fact, we will analyze the LEO operation concept with a range cut-off at 400 km (further called LEO_400) in addition to a range cut-off at 10000 km. For both concepts of the GEO operation we analyze the FoV crossing characteristics with a 10000 km range limit.
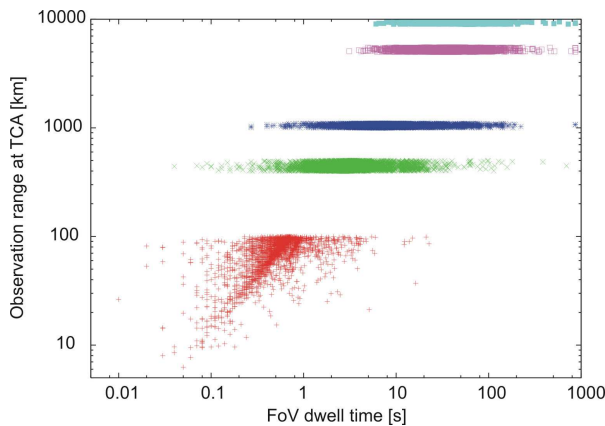
Fig. 5: FoV dwell times in the LEO concept for five selected data subsets with different bands of the observation range.

Table 1 and Table 2 summarize the results of the performance simulation with PROOF. In Table 1 the so-called unique crossings are listed, which are the number of objects that are observed only once within the simulation period, and the number of so-called multiple crossings, which refers to objects that cross the sensor FoV at least twice during the simulation. The large deviation between the number of LEO and GEO FoV crossing events due to the significant differences in the density of the space debris population is visible. Table 1 shows that in the LEO case the majority of the objects cross the FoV multiple times within the simulation period. For the subGEO and GEO most FoV crossing events are unique. The GEO case is worse than the subGEO and LEO case due to the non-optimal phase angle conditions (the North/South pointing leads to average phase angles of 90°).

Table 2 shows that small-sized debris objects are detected, even for the higher SNR detection threshold of 4. In LEO smaller objects compared to the subGEO and GEO cases are observed for a given SNR detection threshold, due to the shorter ranges to the objects. It should be noted that the presented numbers do not yet take into account a possible loss due to failed image processing or orbit determination. It is thus more interesting to assess the number of objects that cross the FoV and for which the objects were detected and the orbit determinations were successful.

We need to add that deviations in the numbers of FoV crossing objects presented in the SBO Final Report [1] can be explained by the different diameter threshold of 5 mm, the use of the new 2005 version of the space debris population model MASTER (the parameters of the GEO fragmentation events and their total number have been revised in MASTER-2005), and the larger considered ranges of 10000 km in the present work. Ranges of 500 km in LEO and 3000 km in GEO were used in the previous work, mainly due to limitations in the computation effort.

	LEO	LEO_400	SubGEO	GEO
Unique FOV crossing events	18906	10829	2595	1619
Multiple time FOV crossing events	48765	10695	162	243

Table 1: Number of FoV crossing objects larger than 5 mm diameter within 576 h simulated observation time for the three considered operation concepts.

	LEO		LEO_400		SubGEO		GEO	
SNR>1	43076	7	6589	7	642	9	254	12
SNR>2	33452	8	5055	8	513	9	198	30
SNR>3	28620	8	4417	8	434	23	163	34
SNR>4	27301	8	4273	8	419	23	157	34

Table 2: Number of FoV crossing objects larger than 5 mm diameter within 576 h simulated observation time for various simulated SNR detection thresholds (peak values per FoV crossing event), together with the related minimum object diameter (in mm) in *italic*.

From Table 2 we calculate a rough estimate for the average detection rate. 7.5 objects/hour are expected in LEO within the 400 km range, if a SNR detection threshold of 4 is assumed. Within the 10000 km range we calculate 47 objects/hour in LEO, 0.7 objects/hour for subGEO, and 0.3 objects/hour for GEO (North/South). The presented rates refer to continuous operations over the full revolution of the sensor. However, in the subGEO the Earth will be in or close to the FoV of the sensor once per revolution and thus only about half of the total mission time can be used for observations.

We continue the discussion of the performance of the proposed instrument and operation concept with a detailed analysis of the main parameters that limit the detection of objects. These parameters for optical observations are:

- the FoV dwell time, which is equivalent to the angular velocity with respect to the FoV taking into account a path offset,

- the brightness of the background, and

- the apparent brightness of the object, determined by range, phase angle, object diameter and albedo.

We consider the exposure time and the instrumental noise as fixed.

We start the discussion of the simulation results with the analysis of the orbital elements of the FoV crossing objects. This allows assessing the coverage of the space debris population with the proposed operation concepts. The plots in Figure 6 and 7 refer to the orbital elements as returned by PROOF.

In Figure 6 semi-major axis a and eccentricity e are given. A reasonable number of GTO objects are crossing the FOV in all concepts, visible as the clustered population at higher eccentricities. Both GEO concepts show similar results, the subGEO case returns additional crossings at about 40'000 km semi-major axis – mainly objects that do not cross the FoV of the North/South pointing GEO telescope.

Inclination i and right ascension Ω of the ascending node are plotted in Figure 7. For the GEO concepts we may distinguish two classes of objects. The first class comprises the GEO objects with an inclination below about 20°. We recognize the well-known pattern in the i-Ω space. Due to the North/South-oriented pointing in the GEO operation concept, there are basically no crossing objects in very low inclination orbits. A second class of objects around 67° could be traced back to MEO objects in the MASTER population with a semi-major axis between approximately 25'000 and 30'000 km crossing the FOV at ranges below 10000 km. For the LEO-400 plot the preferred inclination bands for sun-synchronous and telecommunication satellites can be identified, hence this is the region where most of the small sized debris detections are expected. The LEO plot covering long-range observations shows a good agreement with the modeled space debris environment in LEO, the entire right ascension range is quite uniformly covered and selected inclination bands with higher crossing rates can be identified.
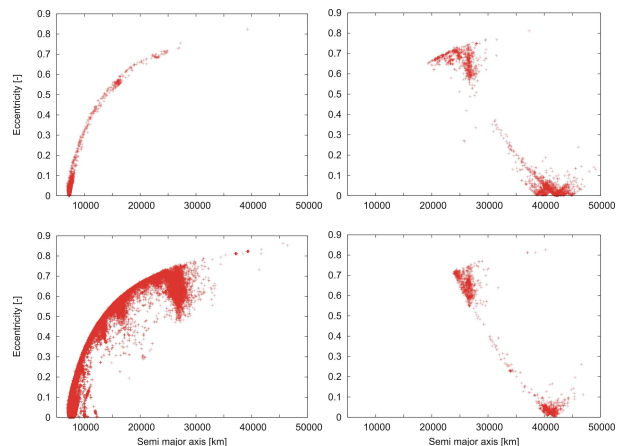
Fig. 6: Eccentricity vs. semi-major axis of the FoV crossing objects larger than 5 mm within the 576 h simulation for LEO-400 top-left, LEO bottom-left, subGEO top-right, GEO bottom-right.
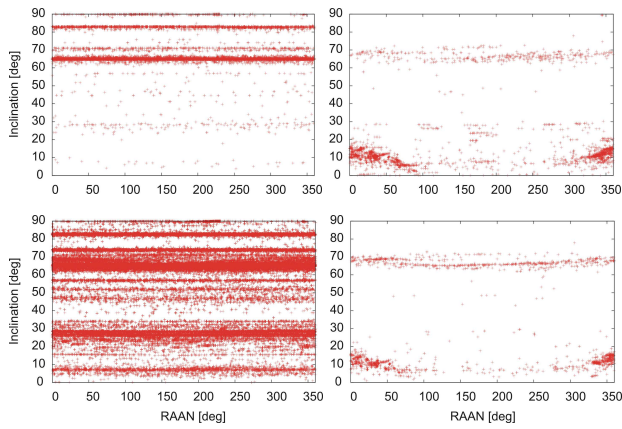
Fig. 7: Inclination vs. right ascension of ascending node of the FoV crossing objects larger than 5 mm within the 576 h simulation for LEO-400 top-left, LEO bottom-left, subGEO top-right, GEO bottom-right.
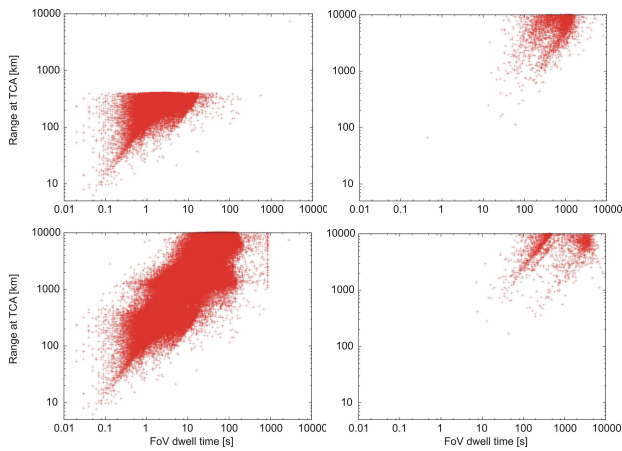
Fig. 8: Minimum range vs FoV dwell time for the simulated LEO, subGEO and GEO operational concepts considering objects larger than 5 mm diameter within 576 h simulated observation time; LEO-400 top-left, LEO bottom-left, subGEO top-right, GEO bottom-right.

Figure 8 compares the expected FoV dwell time for all considered observation concepts. This plot illustrates some of the main problems that relate to the orbit determination. As already pointed out, the dwell times in the LEO operation concept are very short, while in GEO dwell times of several minutes allow the coverage of an arc of sufficient length. In GEO only a few short-range FoV crossings are expected while in LEO the placement of the sensor platform into a densely populated region causes a large number of short-range crossings. The much higher number of expected detections in LEO drives the requirements for the on-board data processing and impacts the data transfer budget.

The apparent brightness of the FoV crossing objects as a function of the brightness of the sky background is given in Figure 9. We conclude that the majority of the objects are very faint objects. In LEO, close objects (within the 400 km range) appear mostly brighter than 15 mag. Without limiting the range, 5 mm objects may appear even fainter as 20 mag. In GEO the largest part of the objects appears fainter than 15 mag. In all cases occasionally brighter objects (as bright as 0 mag in LEO or 5 mag in GEO) may cross the FoV. The instrument is designed to cope with this large dynamic range. All operation concepts allow observations where the sky background is fainter than 20 mag.

Figure 10 shows the phase angle variations as function of the observation epochs. The structure of the plot is spaced by 15 days due to the simulation of 24 h runs. The phase angles are between 0° and 60° in LEO, irrespective of the selected range band. In GEO the average phase angle is comparably worse with 90°, but always between 50° and 130°. Best phase angle conditions are obtained in the subGEO operation concept due to the optimum pointing in right ascension away from the Sun keeping the phase angle below 25°. The phase angles show prominent seasonal variations caused by the varying declination of the Sun. In the GEO operation concepts the variation of the phase angle within 24 h is constant (about 5° in subGEO and 25° in GEO), but the 24 h average of the phase angle shows a one-year variation. In LEO the 24 h average of the phase angle stays constant, but there is a one-year variation of the range within 24 h. The range within 24 h is narrow when the declination of the Sun is low (in spring and autumn), the largest scattering range is expected at high declinations of the Sun. The subGEO operation concept allows for optimal illumination conditions (phase angle is zero) two times a year, when the declination of the Sun equals the inclination of the SBO sensor orbit.

Finally, Figure 11 gives the most important plot for the evaluation of the expected sensor performance – the plot of the simulated peak SNR as function of the object diameter. The analysis reveals for an SNR detection threshold of 4 an average diameter of the FoV crossing objects of about 7 cm for the LEO case and about 10 cm in the two GEO operation concepts. For a given SNR detection threshold the diameter covers a range of about 10 cm. For a SNR of 4 there are detections below 1 cm in LEO and at around 2-3 cm in GEO possible, as Table 2 already showed.

7
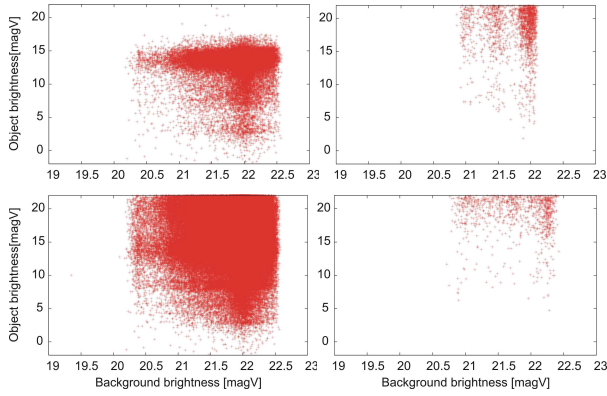
Fig. 9: Brightness of the FoV crossing objects vs the brightness of the sky background for all objects larger than 5 mm diameter within 576 h simulated observation time; LEO-400 top-left, LEO bottom-left, subGEO top-right, GEO bottom-right.
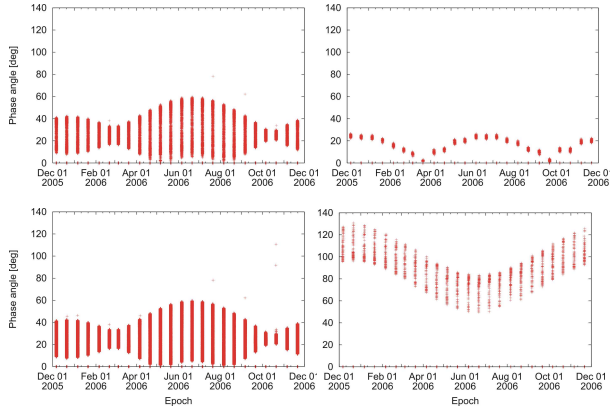
Fig. 10: Phase angle variations as function of the observation epoch; LEO-400 top-left, LEO bottom-left, sub-GEO top-right, GEO bottom-right.
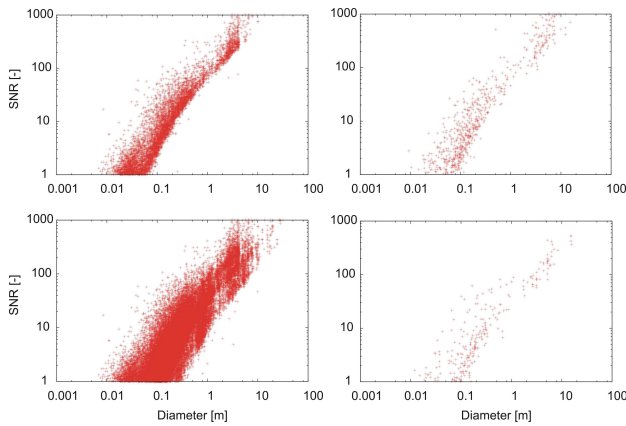
Fig. 11: Peak SNR vs. diameter of the FoV crossing objects larger than 5 mm within the 576 h simulation for LEO-400 top-left, LEO bottom-left, subGEO top-right, GEO bottom-right.

Performance of the image processing

In this section we summarize the results of the evaluation of the image processing algorithms from the SBO Final Report [1]. In order to evaluate the performance of the proposed SBO instrument a large number of test images were generated. The images were simulated with the Image Reduction and Processing Facility (IRAF). The generation of the test images considered the different operation concepts, the sensor architecture, and various FoV crossing angles. The proposed SBO on-board object detection algorithm was applied to the test images. The SBO study concluded that the acquired images should be processed on-board following a "dynamic masking" approach using dedicated image pre-filtering processors. The resulting sub-frames containing stars and possible debris objects (and likely some cosmic ray events, processing artifacts, etc.) should be further processed on-ground. The necessary processing steps are centroiding, astrometric reduction, orbit determination, and estimation of the size of the objects. For the on-ground processing it was proposed to use the border-and-fill algorithm that is used in AIUB's Off-line Data Processing System [14].

In the SBO study a slightly modified implementation of the border-and-fill algorithm was applied in order to precisely discriminate object and background pixel and to determine the centroids of the star and debris objects. A comparison of the determined centroids with the input into the IRAF program system allows to determine the SNR cut-off and also to assess the accuracy of the centroiding procedure afterwards.

The astrometric error is mainly influenced by the centroiding error of star and object, and the epoch registration error. The determination of the centroid of fainter objects close to the SNR limit is of lower accuracy compared to the brighter objects. Thus, the centroiding error was determined as a function of the apparent brightness. The apparent brightness is not only a function of the diameter of the objects. It also depends on the phase angle, the range to the objects, and the shape and surface properties of the objects.

With this approach a limiting apparent brightness of the detection algorithm was found at about 15.6 mag for GEO, 15.8 mag for subGEO and 10.3 mag for LEO using the CCD detector. In the HyViSI detector, the values are 16.0 mag for GEO and subGEO and 10.6 mag for LEO. The limiting

8

magnitude is comparable for the GEO and the sub-GEO operation concept; the faintest objects can be detected in these two concepts. The limiting SNR value is around 4 for the GEO operation concepts and 3 for the LEO operation concept.

Lowering the detection threshold allows the detection of fainter, and thus smaller and more, objects, but produces a higher number of "false" detections. It is an issue of the on-board software implementation and telemetry limitations what false detection rate may be allowed by selecting the SNR detection threshold. We assumed that 95% correct detections must be guaranteed.

Table 3 gives classes of the obtained object centroiding errors in pixel coordinates (Δx and Δy) for the range of possible apparent brightness values. The smallest errors correspond to the brightest objects, the largest errors to objects crossing the FoV at the SNR detection limit. Due to the different proposed operation concepts (mainly the orbital and pointing strategies) the centroiding error covers different ranges. Table 3 also presents the transformation of the centroid determination error into a centroid position error using the pixel scale of the SBO. In the next section we will use these centroiding error classes while simulating position measurements as part of the orbit determination simulation. "Error-free" position measurements can be obtained from the observation geometry at the simulation epoch, but we need to address the instrumental noise sources realistically. The centroiding accuracy derived by the image processing will be used to add normal-distributed noise to the simulated position measurements in the orbit determination simulation.

With the release of PROOF-2005 it became possible to use the synthetic images that PROOF uses internally. User-defined image processing algorithms may replace the PROOF built-in detection criterion, which is basically an SNR detection threshold, by means of a plug-in mechanism. As a first step, we developed a conversion routine in addition to the plug-in that exports PROOF synthetic images in the FITS format. It is thus now possible to directly feed PROOF data into existing image processing facilities like IRAF or AIUB's off-line data processing system. The detailed analysis of the image processing using these PROOF synthetic images directly remains future work.

	Apparent brightness [mag]	Δx, Δy [pix]	Centroiding error["]
LEO	Brightest objects	0.15	1.98
	<8.5	0.4	5.2
	<9.5	0.6	7.9
	<10.5	1.2	16
SubGEO	Brightest objects	0.01	0.13
	<14.5	0.1	1.3
	<15	0.2	2.6
	<15.5	0.3	3.9
	<16	0.4	5.2
GEO	Brightest objects	0.01	0.13
	<11	0.03	0.4
	<12	0.1	1.3
	<14.5	0.4	5.2
	<16	1.2	16

Table 3: Obtained cases for centroiding accuracy (after astrometric reduction step during on-ground processing) in pixel units and maximum corresponding position error in arc seconds, assuming the SBO pixel scale of 9.041"/pixel.

Performance of the orbit determination

The determination of the orbits of the unknown space debris objects is the major objective of the SBO system. For the estimation of the size of the objects from the apparent brightness the range to the objects must be known. The range is computed from the determined objects orbits and the sensor orbit. Both, the (at least statistical) knowledge of the orbital elements and the size of the objects, are the required input into space debris population models.

The performance of the orbit determination of the FoV crossing objects was assessed using an extended version of the ORBDET program, which is part of the CelMech program system [15]. ORBDET provides algorithms for first orbit determination (FOD) and orbit improvement. ORBDET was updated with a new approach for the first orbit determination, and was adapted to support space-based platforms and the output of the observation geometry from the PROOF tool.

For the FOD two approaches were used for all operation concepts, allowing either full-parameter orbit determination or reduced parameter orbit determination. The full-parameter orbit determination was simulated using two "boundary value" approaches. The first boundary value approach (BNBN) is the one used in ORBDET. The second one (BN2D) is a related, but newly developed implementation into ORBDET. Reduced parameter

orbit determination was only simulated for the LEO operation concept. For the reduced parameter approach we used the circular orbit determination algorithm of ORBDET.

Both boundary value approaches follow the idea that two boundary vectors r_a and r_b (geocentric positions of the unknown object at the boundary epochs t_a and t_b) can be calculated from the observed direction between sensor and unknown object and the known sensor position, if the topocentric distances Δ_a and Δ_b are known. As the latter two are obviously not known in the case of optical observations, a systematic variation within given limits is performed. This allows the determination of the "best fit" by minimizing the sum of the residual squares. The residuals between observations and determined orbit are estimated in right ascension and declination. At least 3 observations (in fact astrometric position measurements) are required for the boundary value approach. BNBN makes use of the assumption $r_a \approx r_b$. See [16] for details. The second boundary value approach BN2D allows a two-dimensional search in the Δ_a - Δ_b - space. In this new implementation a filtering mechanism was added that excludes all hyperbolic solutions ($e>1$). In both implementations we make use of all observations that are available. The arc of the entire FoV crossing is considered in the FOD. The solution is thus a two-body orbit, which represents the observations best. In the simulations we use for both, BNBN and BN2D, a search range of 50 km$<\Delta<$12000 km with a step size of 15 km.

Circular orbit determination (e and ω are assumed 0 in the FOD) is possible if two observations are available. ORBDET performs a search in the mean motion space that is determined by given limits of the semi major axis. The algorithm searches for the semi-major axis where the angle between the two position vectors calculated from the observation geometry equals the angle calculated from the particular mean motion. The solution may show ambiguities. See [15] for a detailed outline of the algorithm.

After the FOD an orbit improvement step is carried out that considers the major perturbing forces, the Earth's oblateness and luni-solar perturbations. The orbit improvement includes a least squares adjustment that uses all given (simulated) observations. A discussion of orbit determination results using the obtained RMS, and the residuals is therefore possible.

We start the simulation with the output from PROOF. The plug-in provides the observation geometry for the simulated exposure epochs in addition to the arrays containing the pixel coordinates and the according charge of the object and star signal, and the background signal. The output data combines the epoch, the position of the sensor, and the position and velocity of the observed object. Unfortunately, it is not directly possible to trace the output observation geometry back to the simulated FoV crossing characteristics. This missing functionality of the plug-in would be needed to assign directly a specific astrometric error as function of the simulated brightness and FoV crossing velocity to the simulated orbit determination. ORBDET processes the data from the PROOF-plug-in, and simulates astrometric observations (pairs of right ascension and declination of the objects centroid) for all epochs. Noise is added that reflects the astrometric error and the error in the determination of the sensor position.

We consider all FoV crossing objects in the simulation of the orbit determination, irrespective of their FoV crossing characteristics. Especially it is ignored at this point, whether the SNR allows for a detection, or not. This approach allows us to discuss the performance of the orbit determination with a larger number of events. We will combine the orbit determination results with the results from the simulation of the image processing and the characteristics of the FoV crossing afterwards.

The SBO study concluded that using HyViSI detectors millisecond accuracy is possible for the epoch registration. It is therefore assumed that the contributions from the epoch registration accuracy to the overall error budget are contained in the range of the considered astrometric error. No additional epoch registration error was added to the simulated observations. The astrometric error was included as function of apparent brightness (Table 3). Therefore the simulation of the orbit determination covers 4 classes in LEO, and 5 classes in subGEO and GEO.

Today, the position of satellites can be determined without special means to better than 2 m in LEO, and 10 m in GEO. Thus, a random normal distributed noise with a 1-σ error of 10 m in each of the 3 axes in subGEO and GEO operation concept, and of 2 m in LEO was added to the position of the observing platform.

10

We will now discuss the results of simulated orbit determination for a subset of the PROOF-data: 24 h of observation at epoch 2006-06-12.

In total the orbit determination from 38572 FoV crossing events in the LEO concept, 510 in the sub-GEO concept and 293 in the GEO concept was simulated. With the assumption of a 1 s image acquisition rate about 10% of the FoV crossing events in LEO do not give enough observations. In the case of circular orbit determination this applies to only about 2% of the events. In the GEO and subGEO concept basically all events give a sufficient number of observations for a full orbit determination.

The orbit determination algorithm does not always succeed. Hyperbolic orbits may be determined, or the determined first orbit may not be good enough as input for the orbit improvement step. The number of not successful orbit determinations attempts increases with the astrometric error of the position measurements. BN2D is more successful in determining first orbits than BNBN is. BN2D successfully solves about 90% of the cases in all three considered concepts. This is due to the exclusion of hyperbolic orbits prior the orbit improvement step. BNBN has a performance of about 50% in LEO and about 80% in subGEO and GEO.

All successful orbit determinations may be characterized and classified according to the reached accuracy by comparing the determined orbital elements with the "true" elements provided by PROOF.

A crucial point is the definition of the acceptance criteria. For our simulation, we rate an orbit determination as "accepted", if the difference between "true" and "determined" is smaller than

- 500 km in semi-major axis a, 0.05 in eccentricity e, 5° in inclination i, and 5° in right ascension of the ascending node Ω (applied in the LEO case), or

- 1000 km in semi-major axis a, 0.1 in eccentricity e, 2° in inclination i, and 2° in right ascension of the ascending node Ω (applied in the subGEO and GEO case).

The FOD from the expected short observed arcs must be considered as difficult. Figure 12-14 show the results of the comparison between "true" and determined orbital elements for the different FOD algorithms. The value 100% refers to all successful FOD attempts.

From the plots we may conclude that in all cases and for all used algorithms, the performance of the orbit determination only slightly degrades with increasing astrometric error. This means that orbits of faint objects can be determined with nearly the same quality as orbits for bright objects.

In LEO the circular orbit determination outperforms both boundary value approaches. The determination of Ω is the weakest. The determination of a, e, and i is accepted in about 40% of the successful FODs.

In the subGEO case, the BN2D algorithm fails to find the correct minima, which yields a very low performance. The BNBN algorithm determines the shape of the orbit (a, e) in more than 80% of the successful FODs and the orientation of the orbital plane (i, Ω) in more than 60% of the successful FODs.

The results for the GEO show a comparable good performance for both, BNBN and BN2D. The shape of the orbit (a, e) is better determined than the orientation of the orbit (i, Ω). The determination of the shape is accepted in 60-80% of the successful FODs, while the orientation of the orbit is accepted only in 40-50%. BNBN performs slightly better for the fainter objects than BN2D, but the total number of successful FODs is higher for BN2D.

A detailed analysis of the not accepted FODs showed that mostly the highly elliptical orbits ($e>0.3$) are difficult to determine. As these orbits are not of prime interest for the SBO system (the focus is on small objects in LEO and GEO and thus on more circular orbits), we may exclude these objects after the orbit determination. A simple perigee/apogee height criterion using the determined perigee and apogee values turned out to be suitable for first tests.

The used a posteriori filter was:

- minimum perigee height of 6500 km and maximum apogee height of 15000 km in LEO,

- minimum perigee height of 30000 km and maximum apogee height of 60000 km in subGEO and GEO.
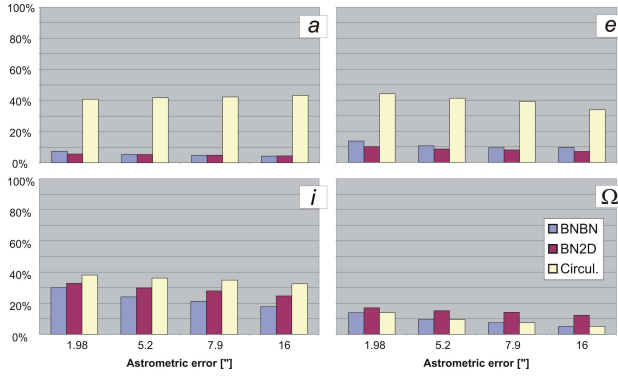
Fig. 12: LEO case, percentage of 'accepted' FODs with respect to the total number of successful FODs, acceptance criteria: 500 km for *a*, 0.05 for *e*, 5° for *i*, and 5° for Ω.
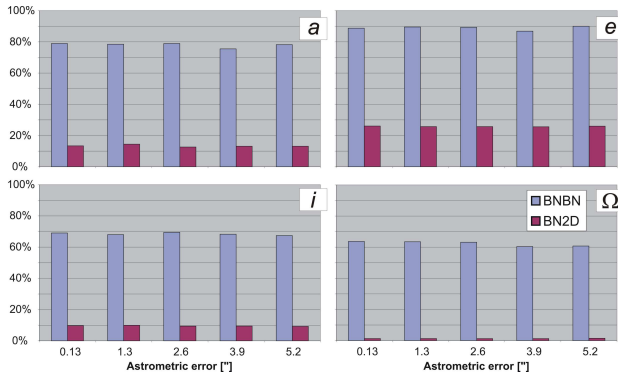
Fig. 13: SubGEO case, percentage of 'accepted' FODs with respect to the total number of successful FODs, acceptance criteria: 1000 km for *a*, 0.1 for *e*, 2° for *i*, and 2° for Ω.
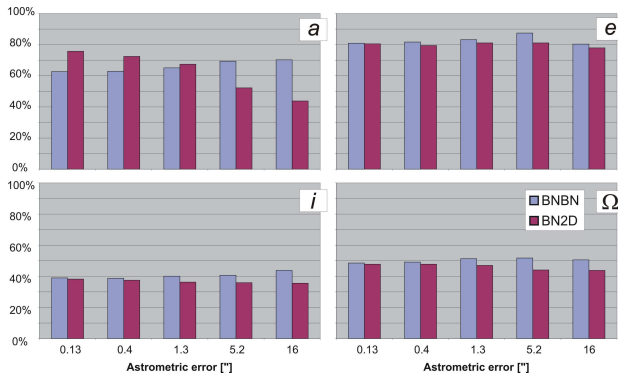
Fig. 14: GEO case, percentage of 'accepted' FODs with respect to the total number of successful FODs, acceptance criteria: 1000 km for *a*, 0.1 for *e*, 2° for *i*, and 2° for Ω.

A test was carried out to ensure that the proposed filtering criteria do not exclude "poorly determined interesting objects". We compared the filtering of the PROOF results (our "truth") against the filtering of the ORBDET output. Only about 1-2% of the objects are wrongly excluded (7 out of 390 in sub-GEO in the worst case, 1 out of 178 in GEO in the worst case). In LEO the number of wrongly excluded objects is by far higher, up to 30%. Thus the filtering in LEO is not reliable.

In analogy to Figure 12-14, Figure 15-17 show the results of the comparison between "true" and determined orbital elements for the a posteriori filtered successful FODs. The acceptance criteria remained unchanged. For all concepts the improvements can be seen in the plots.

In LEO the circular orbit determination still outperforms both boundary value approaches. The most prominent improvement is in *a* and *e*, which shows that the hypothesis of circular orbits is valid for most of the LEO population. The determination of *i* and Ω remains difficult.

In the subGEO case, the BN2D algorithm still fails. The BNBN algorithm is now able to determine the shape of the orbit (*a*, *e*) in about 90% of the successful FODs and the orientation of the orbital plane (*i*, Ω) in about 70% of the successful FODs. This is an improvement of 10% absolute.

The results for GEO are also improved by about 10%. The shape of the orbit (*a*, *e*) is accepted in about 90% of the successful FODs, the orientation of the orbit in more than 50%.

We conclude that an a posteriori filtering based on perigee and apogee altitude is recommended for the SBO operation in subGEO and GEO. With the BNBN algorithm, the shape of the orbit can be determined with an acceptable accuracy in most of the cases where the FOD was successful. The determination of the orientation of the orbital plane with the assumed accuracy of 2° mostly succeeds in the subGEO, and succeeds in the GEO in every second case. The determination of a full orbit in the LEO is difficult. But with the determination of circular orbits (a valid assumption that simplifies the FOD) the shape of an orbit can be determined meeting our acceptance criterion in more than 50% of the successful FODs. The determination of the orientation of the orbits in LEO is difficult due to the very short covered arcs (in the order of seconds) and is thus not very reliable.

12
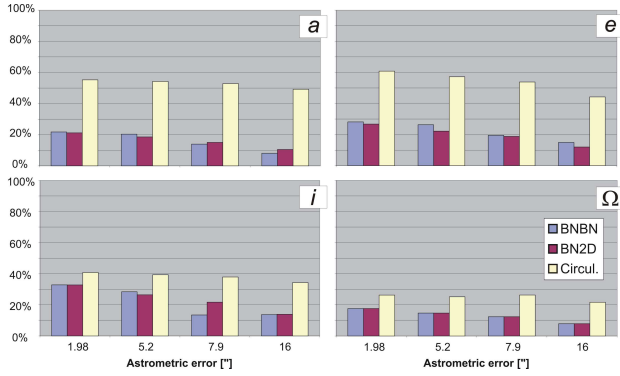
Fig. 15: LEO case, percentage of 'accepted' FODs with respect to the total number of successful FODs (after filtering), acceptance criteria: 500 km for *a*, 0.05 for *e*, 5° for *i*, and 5° for Ω.
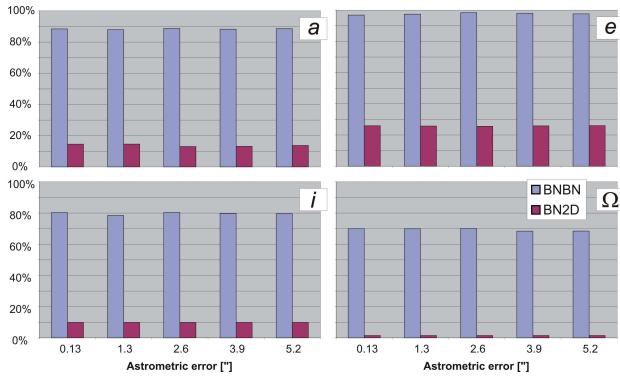
Fig. 16: SubGEO case, percentage of 'accepted' FODs with respect to the total number of successful FODs; (after filtering), acceptance criteria: 1000 km for *a*, 0.1 for *e*, 2° for *i*, and 2° for Ω.
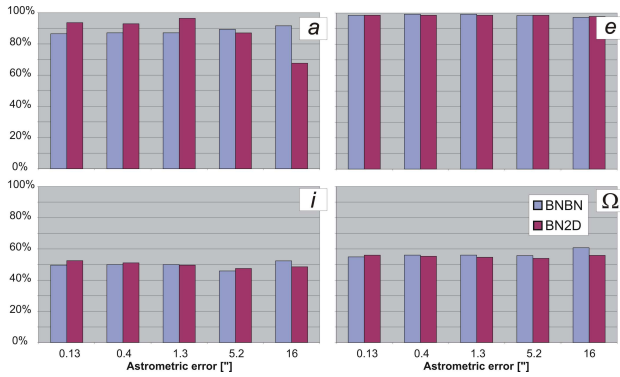
Fig. 17: GEO case, percentage of 'accepted' FODs with respect to the total number of successful FODs; (after filtering), acceptance criteria: 1000 km for *a*, 0.1 for *e*, 2° for *i*, and 2° for Ω.

We further conclude that the RMS criterion is not sufficient to qualify the determined orbit. In sub-GEO and GEO the astrometric accuracy of the position measurements does only slightly impact the quality of the determined orbit. The determined orbits of fainter objects are of a comparable accuracy with those of the brighter objects. In LEO often not enough observations are available for an orbit determination.

The new BN2D approach is an interesting alternative approach in GEO, but there are no benefits of using this algorithm in subGEO and LEO.

Combination of the performance simulation results

The combination of the result from the PROOF analysis with the simulation results for image processing and orbit determination gives the expected numbers of objects for which we may determine orbits.

We follow an approach starting with the application of the detection threshold (peak SNR) as filtering criteria to the list of crossing objects for 576 h of simulated observations. Merging the resulting lists of "objects above the detection threshold" with the orbit determination simulation results (percentage of successful FOD and percentage of accepted FODs) leads to an approximate number of determined orbits. By presenting ranges for these figures we take into account that the orbit determination of fainter objects is slightly more difficult. But we did not, however, assume a real correlation between apparent brightness of a particular object and the orbit determination. We present the statistics for 24 h of observation, knowing that in subGEO observations are not possible throughout the entire revolution of the sensor, and that some observation time is dedicated to calibration issues. The number of objects is given for different classes of object diameter.

A significant assumption in the combination is the number of position measurements provided by the image-processing algorithm. The wide range of different processing issues (star occultations, extended background sources, streak length, ratio between peak and average signal, chosen detector readout approach, adjustment of the centroiding algorithm, etc.) was not covered here. We simply assumed that any FOV crossing event would allow the full image processing and the acquisition of the necessary number of measurements for the orbit

13

determination, if the peak SNR were larger than our estimated value. Already small improvements in the SNR detection threshold would, however, lead to a higher number of detected objects.

Table 4 shows the results of the combination of the performance simulation results. The estimate of objects for which the orbit determination meets the acceptance criteria is given. We use this data as input to Table 5, where we summarize the capabilities of the SBO system and compare with the capabilities of existing ground-based systems. A similar table was already presented in [3]; our new results support the previous conclusions. In LEO ground-based radars are theoretically superior, but due to their limited availability a space-based system could still contribute significantly to the monitoring of the space debris environment. At geostationary altitude (or 1000 km below) the proposed SBO system is clearly exceeding the capabilities of 1-m telescopes on ground. The SBO would enhance the knowledge about space debris by decreasing the minimum object size from about 15 cm to less than 5 cm.

	LEO	SubGEO	GEO
Accepted determination of (a, e) [d^{-1}]	500-600	12-13	4-6
Accepted determination of (i, Ω) [d^{-1}]	200-300	10-12	3
Size of 'accepted' objects	1% smaller than 5 cm,	3% smaller than 5 cm,	1% smaller than 5 cm,
	5% smaller than 10 cm,	12% smaller than 10 cm,	5% smaller than 10 cm,
		41% smaller than 20 cm	26% smaller than 20 cm

Table 4: Expected numbers of objects for orbit determination meeting the acceptance criteria.

	SBO LEO	SBO subGEO	SBO GEO	TIRA Radar (FGAN)	ESA Space Debris Telescope.
Minimum detected object diameter	0.8 cm	2.3 cm	3.4 cm	2.1 cm (1000 km altitude)	~15 cm (at GEO)
Expected detections between 2 cm and 10 cm [d^{-1}]	25-30	1.5-1.6	0.2-0.3	~400	0
Sensor availability	24 h/d	>12 h/d	24 h/d	24 h once or twice per year	~12 nights within 30 days
Orbit determination	Circular	Full para-meter	Full para-meter	Circular	Circular or full para-meter
Tracking capability	No	No	No	Yes[*]	Yes, limited

Table 5: Capabilities of the SBO compared to existing ground-based sensors ([*]stare-and-chase mode for TIRA is under development).

CONCLUSION

We evaluated the system performance of a proposed instrument architecture for the space-based optical observation of space debris. The evaluation involved the analysis of the characteristics of the FoV crossing objects, the estimation of the limits of the image processing based on simulated images, and the simulation of the first orbit determination and orbit improvement.

The detection of small-sized space debris (smaller than 1 dm in diameter) is possible using the sensor architecture and operation scenario proposed in the ESA-study "Space-Based Optical Observation of Space Debris". All of the three operation concepts were evaluated, LEO, subGEO and GEO. In LEO the highest detection rate is expected; small-sized space debris objects are mostly observed with sufficiently high SNR at short ranges. The proposed operation concepts provide dark sky background conditions better than 20 mag. Seasonal variations in the detection efficiency are expected due to varying phase angle conditions. Best phase angle conditions are provided by the subGEO operation concept, fair conditions by the LEO operation concept and moderate phase angle conditions by the GEO observation concept. First orbits with an acceptable accuracy can be determined from a single FoV crossing event in all three concepts, but not for all detections. Ranges for the number of successful orbit determinations within 24 h are given assuming different astrometric errors. From the determined orbits of unknown objects, the object diameter can be determined using the observed apparent brightness. We conclude that placed in LEO the proposed instrument could contribute significantly to the monitoring of the space debris environment; placed at GEO altitude the instrument could decrease the current minimum observed object diameter to less than 5 cm. The instrument would allow improving the knowledge about the uncatalogued small-sized space debris population in LEO and GEO by using a relatively simple and straightforward instrument design and processing strategy.

The ESA PROOF tool in its new version 2005 was used as an extremely valuable tool not only for observation forecasting. PROOF-2005 supports the performance evaluation by providing synthetic images and the corresponding observation geometry. With these functionalities, PROOF becomes useful for further studies, such as the discussion of image processing, and orbit determination algorithms for

particular object categories of statistical or catalogued populations.

REFERENCES

[1] E. Valtonen, J. Peltonen, E. Riihonen, T. Eronen, T. Flohrer, T. Schildknecht, E. Stöveken, F. Wokke, A. Kramer, and R. van Benthem. Space-based optical observation of space debris - Final report, Ed. T. Flohrer, ESA/ESOC, Contract 17140/03/D/HK, 2006.

[2] F.J.P. Wokke, A.J. Kramer, R. van Benthem, R.B. Annes, T. Flohrer, T. Schildknecht, E. Stöveken, E. Valtonen, J. Peltonen, E. Riihonen, T. Eronen, J. Kuusela. An instrument design for space-based optical observation of space debris, Proceedings of the International Academy of Astronautics Space Debris and Space Traffic Management Symposium 2005, American Astronautical Society, 2006 (accepted for publication).

[3] T. Flohrer, J. Peltonen, A. Kramer, T. Eronen, J. Kuusela, E. Riihonen, T. Schildknecht, E. Stöveken, E. Valtonen, F. Wokke, and W. Flury. Space-based optical observations of space debris, Proceedings of the 4th European Conference on Space Debris 18-20 April 2005, ESOC, Darmstadt, Germany, ESA SP-587, 165-170, 2005.

[4] J. Bendisch, J.P. Hoffmann, R. Leibscher, and F. Rollenhagen, Detection of Space Debris by the use of Space Based Optical Sensors, Proceedings of the 1st European Conference on Space Debris, ESA SD-01, 91-97, 1993.

[5] D.R. Lobb, J.S.B. Dick, and S.F. Green. Development of concepts for detection and characterisation of debris in Earth orbit using passive optical instruments, Adv. Space Res., 13, 59-63, 1993.

[6] M. Oswald, H. Krag, P. Wegener, B. Bischof, Concept for an Orbital Telescope Observing the Debris Environment in GEO, Advances in Space Research, 34, 1155-1159, 2004.

[7] F. Alby, G. Otrio and C. Durin, Space Based Observations of Orbital Debris, Space Debris 2000, San Diego, Ed. J. Bendisch, AAS Science and Technologies Series, 103, 35-49, 2001.

[8] OSDT Team, Optical Sensor for Debris Tracking, Executive Summary, ESA/ESTEC, Contract 17324/03/NL/PG, 2005.

[9] E.M. Gaposchkin, C. von Braun, and J. Sharma. "Space-Based Space Surveillance with the Space-Based Visible", Journal of Guidance, Control and Dynamics, 23, 148-152, 2000.

[10] D. C. Harrison and J. C. Chow, The Space Based Visible Sensor, John Hopkins APL technical digest, 17, 226-236, 1996.

[11] H. Krag, M. Kahl, J. Bendisch, H. Klinkrad, T. Schildknecht, Space Based Optical Observation of Small Debris Objects, Proceedings of the 3rd European Conference on Space Debris 19-21 March 2001, ESOC Darmstadt, Germany, ESA SP-473, 147-152, 2001.

[12] H. Krag, A Method for the Validation of Space Debris Models and for the Analysis and Planning of Radar and Optical Surveys, PhD thesis, Shaker publisher, Aachen 2003.

[13] M. Oswald, C. Wiedemann, P. Wegener, S. Stabroth and P. Vörsmann, Accuracy of Space Debris Orbit Determination Using Space-Based Optical Sensors, Space Debris 20033, San Diego, Ed. J. Bendisch, AAS Science and Technologies Series, 109, 77-95, 2004.

[14] T. Schildknecht, U. Hugentobler, A. Verdun, and G. Beutler, CCD Algorithms for Space Debris Detection, Final Report, ESA/ESOC Contract No. 10623/93/D/IM, 1995.

[15] G. Beutler, Methods of Celestial Mechanics, 2 Volumes, Springer, 2005.

[16] G. Beutler, T. Schildknecht, U. Hugentobler, W. Gurtner, Orbit determination in satellite geodesy, Adv. Space Res., 31, 1853-1868, 2003.

[17] M. Oswald, S. Stabroth, C. Wiedemann, P. Wegener, C. Martin, Upgrade of the MASTER Model – Final Report, ESA/ESOC, Contract 18014/03/D/HK(SC), 2006.

[18] M. Oswald, C. Wiedemann, H. Krag, J. Rosebrock, T. Schildknecht, Program for Radar and Optical Observation Forecasting – Final Report, ESA/ESOC, Contract 18014/03/D/HK(SC), 2006.